JOURNAL OF APPLIED PHYSICS **115**, 034513 (2014)

Lateral carrier diffusion and current gain in terahertz InGaAs/InP double-heterojunction bipolar transistors

Han-Wei Chiang, Johann C. Rode, Prateek Choudhary, and Mark J. W. Rodwell
Department of Electrical and Computer Engineering, University of California, Santa Barbara, California 93106, USA

(Received 19 December 2013; accepted 5 January 2014; published online 17 January 2014)

The DC current gain in $In_{0.53}Ga_{0.47}As$/InP double-heterojunction bipolar transistors is computed based on a drift-diffusion model, and is compared with experimental data. Even in the absence of other scaling effects, lateral diffusion of electrons to the base Ohmic contacts causes a rapid reduction in DC current gain as the emitter junction width and emitter-base contact spacing are reduced. The simulation and experimental data are compared in order to examine the effect of carrier lateral diffusion on current gain. The impact on current gain due to device scaling and approaches to increase current gain are discussed. © *2014 AIP Publishing LLC*.
[http://dx.doi.org/10.1063/1.4862405]

I. INTRODUCTION

InP-based npn-double-heterojunction bipolar transistors (DHBTs) are strong candidates for mixed-signal ICs, high speed digital logic, millimeter-wave communications, and imaging and sensing at far-infrared wavelengths due to their high cutoff frequencies and high breakdown voltages.[1–3] Mesa DHBTs with $f_\tau/f_{\max} \approx 0.5/1$ THz have been recently reported.[4,5] The reductions in carrier transit times and parasitic *RC* delays necessary for such bandwidths have been achieved via epitaxial and lateral scaling.[1] However, when the emitter-base junction dimensions of DHBTs are decreased, lateral transport effects at the junction edges become more significant and the DC current gain, β, decreases. Experimentally, $\beta \approx 20$ and 10 are observed at 200 and 75 nm emitter junction widths, respectively. This low current gain is undesirable, limiting the range of useful circuit applications. Thus, understanding the causes of current gain degradation is important to the design of future scaling generations of high-frequency DHBTs.

In HBTs, electron recombination at the exposed base surface adjacent to the emitter contributes significant base current,[6] which can be reduced by introducing a surface junction ledge.[7] In highly scaled THz HBTs, the base-emitter contact spacing is comparable to the base thickness, and significant base current also arises from electrons diffusing laterally to the base contact, where the electrons then recombine. In this paper, we model the resulting variation in DC current gain with HBT geometry. Because the focus of this study is electron recombination at the contacts, the effect of surface recombination is explicitly neglected. Using a commercial simulator, carrier transport in the base region is computed using a drift-diffusion model, calculated at a current density which experimentally gives peak $f_\tau/f_{\max}$. We compare simulations to experimental data, and compute the variation of current gain with emitter width, emitter-base spacing, and base bandgap grading. As the lateral diffusion current cannot be adequately suppressed by a ledge without increasing the base-emitter spacing to the point where $f_{\max}$ is significantly reduced, we then present other techniques to enhance β.

II. SIMULATION PARAMETERS AND EXPERIMENTAL CONDITIONS

The simulations model experimentally fabricated devices. The experimental devices were grown by molecular beam epitaxy (MBE) on a (001) InP substrate. Mesa DHBTs with self-aligned base-emitter junctions were fabricated using the process flow of Jain.[4] DC characteristics were measured using an Agilent 4155 C semiconductor parameter analyzer.

Fig. 1 shows DHBT schematic cross section. Because of the reaction of the Pt base contact metal with the base,[8] there is a vertical offset, $T_{\text{B, Sink}}$, between the base-emitter metallurgical junction, and surface of the base contact. From our TEM analysis, $T_{\text{B, Sink}} \simeq 5$ nm. In the HBTs here considered, emitter stripe length (L_E) $\gg$ width (W_E), hence base current is dominated by contributions from bulk and from the sides of the emitter-base junction, and we will neglect the non-dominant contribution from base recombination currents at the ends of the emitter stripe. While the experimental devices have wide-bandgap InP collectors, the simulations assume an InGaAs collector and sub-collector. This simplifies simulation and does not significantly change the computed DC current gain because the boundary condition between the undepleted base and the depleted collector is not changed when the collector current density is lower than the Kirk-effect-limited current density[9] (J_{Kirk}),

$$J_{\text{Kirk}} = qn_d v_{\text{sat}} + \frac{2\epsilon v_{\text{sat}}}{T_C^2}(V_{CB} + \phi), \tag{1}$$

where n_d is the collector doping, v_{sat} the mean electron velocity in the collector, T_C the collector thickness, V_{CB} the collector-base bias voltage, and ϕ the junction built in potential. Therefore, the setback, base-collector grade, and InP collector of the experimental DHBT were replaced in the simulations by an n-InGaAs layer having a similar electric field to that of the setback layer. The layer structure of the simulated HBT is listed in Table I.

The HBT current gain was computed using Synopsis® Sentaurus whereby the coupled continuity, drift-diffusion,

 © 2014 AIP Publishing LLC

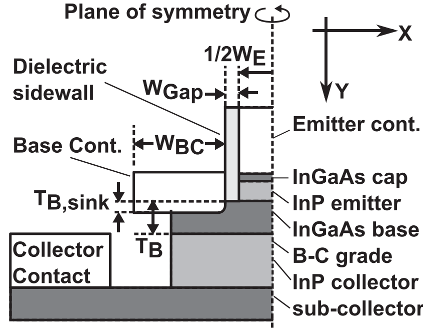

FIG. 1. Schematic cross section (normal to the emitter stripe) of experimental DHBTs. The device is symmetric about the indicated line; hence only half is shown.

and Poisson's equations were self-consistently solved. In the simulation, the doping-dependent carrier mobilities at low field are extrapolated according to the Caughey-Thomas model[10]

$$\mu(N) = \frac{\mu_{\max} - \mu_{\min}}{1 + (N/N_{\mathrm{ref},\mu})^{\alpha}} + \mu_{\min}, \tag{2}$$

where $N_{\mathrm{ref},\mu}$ is a reference (low) doping level, and $\mu_{\min}$ and $\mu_{\max}$ are the minimum and maximum mobilities at high and low doping levels, respectively. In our simulation, $N_{\mathrm{ref},\mu}$ was set to the conduction-band effective density of states. Diffusion under either high electric fields or large diffusion gradients was modeled according to $v_{\mathrm{drift}} = \mu_{\mathrm{highfield}} F$, where[11]

$$\mu_{\mathrm{highfield}} = \frac{\mu_{\mathrm{lowfield}}}{\left(1 + \left(\frac{\mu_{\mathrm{lowfield}} F}{v_{\mathrm{th}}}\right)^{\gamma}\right)^{1/\gamma}}, \tag{3}$$

where $F = q^{-1} dE_{\mathrm{fn}}/dy$ is the quasi-field driving electron transport and E_{fn} the electron quasi-Fermi level. γ is set to 10 to ensure a rapid transition from low-field to high-field mobility, as is observed in the InGaAs/InP system.[12]

In the HBT's graded base, carrier transit time, τ_B, is

$$\tau_B = \frac{T_B^2}{D_n}\frac{kT}{\Delta E_C}\left[1 - \frac{kT}{\Delta E_C}\left(1 - \exp\left(-\frac{\Delta E_C}{kT}\right)\right)\right] + \frac{T_B}{v_{\mathrm{exit}}}\frac{kT}{\Delta E_C}\left(1 - \exp\left(\frac{\Delta E_C}{kT}\right)\right), \tag{4}$$

where $D_n = \mu_n kT/q$ is the electron diffusivity, T_B the base thickness, and ΔE_C the conduction-band potential difference across the base region.[13] The DHBTs considered here have a 20 nm doping-graded base design similar to that of Jain,[4] where the base thickness is 30 nm and ΔE_C is determined by the doping gradient and by doping-induced bandgap narrowing (BGN). Although ΔE_C can be computed from the doping profile, the base In/Ga ratio has also been varied with position in the base to compensate for the effect of the high doping concentration on the crystal lattice constant. Given these complications, we cannot estimate ΔE_C with confidence in our device, and hence current gain was instead simulated for ΔE_C varying from 54 meV (zero BGN) to 0 meV.

TABLE I. Layer structure of the simulated SHBT.

Layer	Semiconductor	Thickness (Å)	Doping (cm^{-3})
Emitter	InP	150	5×10^{19}:n
Emitter	InP	150	2×10^{18}:n
Base	$In_{0.53}Ga_{0.47}As$	200	$12-8 \times 10^{19}$:p
Collector	$In_{0.53}Ga_{0.47}As$	200	5×10^{16}:n
Sub-collector	$In_{0.53}Ga_{0.47}As$	200	2×10^{19}:n

Three recombination mechanisms in bulk InGaAs were incorporated into the simulation for β: Auger, Shockley-Read-Hall (SRH), and radiative recombination. The overall carrier lifetime due to these processes follows Matthiessen's rule. The Auger recombination rate is given by

$$R_{\mathrm{Auger}} = (C_{\mathrm{Auger,n}} n + C_{\mathrm{Auger,p}} p)(np - n_{\mathrm{i,eff}}^2) \approx C_{\mathrm{Auger,n}} n^2 p + C_{\mathrm{Auger,p}} p^2 n, \tag{5}$$

where $C_{\mathrm{Auger,\ n}}$ and $C_{\mathrm{Auger,\ p}}$ are the Auger coefficients. Values of $3.6-9 \times 10^{-29}$ cm^6/s for $(C_{\mathrm{Auger,n}} + C_{\mathrm{Auger,p}})$ and 3.8×10^{-29} cm^6/s for $C_{\mathrm{Auger,\ p}}$ have been reported.[14–16] In our simulation $C_{\mathrm{Auger\ p}}$ is set to 2.5×10^{-29} cm^6/s in order to obtain the best fit to the experimental data. In the heavily doped p-InGaAs base, $\tau_{\mathrm{Auger}} = n/R_{\mathrm{Auger}} \simeq 1/C_{\mathrm{Auger,p}} p^2 \simeq 2.9$ ps, and Auger recombination is the dominant bulk recombination mechanism. The carrier lifetime due to SRH recombination and its doping dependency were modeled by the Scharfetter relation, with coefficients drawn from experimental data[14,17]

$$\tau_{\mathrm{doping}}(N_A + N_D) = \frac{\tau_{\mathrm{ref}}}{1 + \left(\frac{N_A + N_D}{N_{\mathrm{ref},\tau}}\right)^{\kappa}}, \tag{6}$$

where $N_{\mathrm{ref},\tau}$ is a reference doping level and τ_{ref} the corresponding SRH lifetime. Finally, radiative recombination varies as $C_{\mathrm{rad.}}(np - n_{\mathrm{i,eff}}^2)$[18] with a coefficient $C_{rad.}$ of 9.6×10^{-11} cm^3/s.

Table II gives both the InGaAs parameter values used in the simulation, and the references from which these parameters were determined.

III. RESULT AND DISCUSSION

HBT base current consists of current $I_{\mathrm{B,\ Bulk}}$ arising from recombination process in the bulk (intrinsic) base region, and surface current $I_{\mathrm{B,\ Edge}}$ contributed by both surface recombination and lateral carrier diffusion from emitter edge to the base metal contact. $I_{\mathrm{B,\ Edge}} = K_{\mathrm{B,\ Edge}} P_{je}$ is proportional to the junction periphery, $P_{je} = 2(L_E + W_E)$, where $K_{\mathrm{B,\ Edge}}$ is the component of the base current density proportional to the junction periphery. The current gain can then be written as a function of W_E

$$\frac{1}{\beta} = \frac{I_{\mathrm{B,Bulk}} + I_{\mathrm{B,Edge}}}{I_C} = \frac{1}{\beta_{\mathrm{Bulk}}} + \frac{P_{je} K_{\mathrm{B.Edge}}}{A_{je} J_C} \approx \frac{1}{\beta_{\mathrm{Bulk}}} + \frac{2K_{\mathrm{B.Edge}}}{W_E J_C}, \tag{7}$$

TABLE II. $In_{0.53}Ga_{0.47}As$ parameter values used in simulation and corresponding references.

Parameter	Carrier type		unit
	Electrons	Holes	
μ_{min}[17,19]	1600	75	$cm^2/V-s$
μ_{max}[17,19]	11600	331	$cm^2/V-s$
$N_{ref,\mu}$[17,19]	2.1×10^{17}	7.7×10^{18}	cm^{-3}
α[17,19]	0.76	1.37	
γ	10	10	
τ_{ref}[17]	50	400	ps
$N_{ref,\tau}$[17]	1×10^{19}	1×10^{19}	cm^{-3}
κ[17]	0.73	1.2	
C_{Auger}[14–16]	2.5×10^{-29}	2.5×10^{-29}	cm^6/s
$C_{rad.}$[18]	9.6×10^{-11}		cm^3/s

where $A_{je} = W_E L_E$ is the base-emitter junction area, and where the approximation holds if $L_E \gg W_E$. The current gain β_{Bulk} of an HBT with a very wide emitter is the ratio of electron lifetime to base transit time is $\beta_{Bulk} = \tau_n/\tau_B$.

In HBTs with narrow emitters, surface recombination currents will reduce the DC current gain. In THz HBTs, for low base resistance the base-emitter spacing is also small, and base current arising from recombination at the base contacts is also significant. To obtain high current gain, both surface recombination and base contact recombination must be suppressed. It is the intent of this study to determine the magnitude of the base contact recombination. Surface recombination was therefore set to zero in simulation.

Fig. 2 compares simulations to experimental data. DC current gain is computed as a function of emitter periphery/area ratio P_{je}/A_{je}, as a function of the spacing W_{gap} between the emitter-base junction and the base contact, for base grading (difference in the base conduction-band potential at the emitter-base and base-collector junctions) of ΔE_C of 54 meV, 22 meV, and 0 meV, and for base contact width $W_{BC} = 1.2W_E$, $1.4W_E$, and $1.6W_E$. The dashed lines are the least-square linear fit to the simulations for each W_{gap}, from which the bulk current gain β_{Bulk} was extrapolated.

In the experimental devices, the collector current density reaches the Kirk effect limit when $V_{CB} \simeq 0.6$ V and the emitter current density $J_E > 25\,mA/cm^2$. Peak RF performance is observed at the current density only slightly below the Kirk effect limit. The experimental DC current gain data of Fig. 2 is therefore plotted at an emitter current density $J_E \simeq 25\,mA/cm^2$. In the experimental data, the variation of current gain with emitter periphery/area ratio suggests $\beta_{Bulk} \simeq 45$ and $K_{B,\ Edge} \simeq 72\mu A/\mu m$. TEM images of the fabricated devices indicated $W_{gap} \simeq 10$–20 nm. As is also seen in Fig. 2, increasing the base grading ΔE_C increases the DC current gain. Bulk recombination is reduced because of decreased base transit time, and hence a larger ratio of Auger lifetime to base transit time, while current gain at small emitter widths (large P_{je}/A_{je}) is increased by the increased vertical electric field driving carriers away from the contacts. As noted earlier, bandgap narrowing reduces the base field produced by base doping grading. Given the doping grading employed in Table I, in the absence of BGN, ΔE_C would be 54 meV. Simulation were also performed for HBTs

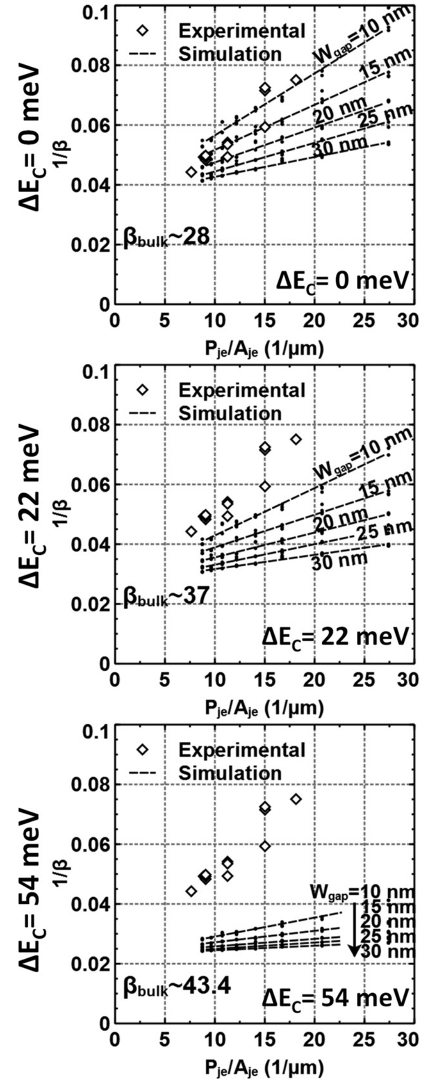

FIG. 2. Inverse DC current gain ($1/\beta$) vs. HBT emitter periphery to area ratio (P_{je}/A_{je})for base conduction band potential grading (ΔE_C) of 0, 22, and 54 meV, base emitter spacing (W_{gap}) of 10, 15, 20, 25, and 30 nm. The effect of surface recombination is neglected. Current gain was simulated for base contact width of 1.2 W_E, 1.4 W_E, and 1.6 W_E.

with 5 nm of base contact penetration depth (into InGaAs) due to the reaction between Pt and InGaAs,[8] as is observed from HBT TEM cross sections of the experimental devices. However, the effect in simulation of base contact sinking on current gain is small for HBT dimensions similar to that of the experimental devices.

Beyond the effect of emitter width itself, most significant in the data of Fig. 2 is the decrease in DC current gain with decreased base-emitter spacing W_{gap}. Examining the case of $\Delta E_C = 22$ meV and 5 nm base contact sinking, at the simulated $J_E = 25\,mA/\mu m^2$, $K_{B,\ Edge}$ varies from 43 $\mu A/\mu m$ for a 10 nm base-emitter gap to 12 $\mu A/\mu m$ for a 30 nm base-emitter gap. With these parameters, with a 100 nm emitter junction width, the simulated DC current gain β decreases from 26.1 at $W_{gap} = 30$ nm to 15.4 at $W_{gap} = 10$ nm.

Although β can be increased by increasing W_{gap}, doing so also increases base access resistance, R_{bb}, and thereby decreases the transistor power-gain cutoff frequency f_{max}.

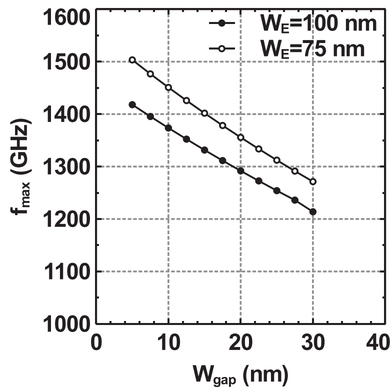

FIG. 3. HBT power gain cutoff frequency, f_{max}, calculated according to method of[1] as a function of emitter-base spacing W_{gap} and emitter width W_E.

Assuming[1] a collector thickness of 75 nm, emitter and base contact resistivities of 4 and 5 Ω-μm^2, a base contact width equal to the emitter width, and assuming an operating current density of 36 mA/cm^2, Fig. 3 shows the calculated HBT f_{max} as a function of W_{gap} in HBTs at emitter junction widths of 100 nm and 75 nm. At 100 nm emitter width, the base resistance added by 30 nm base-emitter contact spacing decreases f_{max} by $\sim$14%.

In these simulations, DC current gain decreases rapidly as the emitter junction width and base-emitter spacing are reduced, decreasing to current gains as small as $\beta = 15$ at 100 nm emitter contact width and 10 nm base-emitter spacing. With surface recombination neglected, the computed decrease in current gain entirely results from carrier recombination at the base contacts. Carrier recombination at the base contacts plays an important role in the degradation of current gain, and will become progressively more significant as the junctions scale further in future HBT generations.

To obtain high β for HBTs with the sub-100 nm emitter widths and sub-30 nm base-emitter contact spacings required[1] for $f_{max} \simeq 1.5$–2.0 THz, excess base currents from surface and base contact recombination must be reduced or suppressed. Increasing the vertical driving force $(q^{-1}dE_{fn}/dy)$ in the base through either reduced base thickness or increased base grading will reduce both surface and base contact recombination currents. Considerations here include the increased sheet resistance of thin base layers, increased Auger recombination with high base doping levels associated with strong base doping gradients, and complications with both strain and dopant incorporation in HBT designs using strong base bandgap grading.[20] Another approach for increased β is epitaxial base regrowth; in Si/SiGe HBTs,[21] extrinsic and very heavily doped P+ polysilicon layers are grown above the more lightly doped intrinsic base adjacent to the emitter-base junction. The large doping differential between the intrinsic and extrinsic base produces a large field inhibiting electron transport to the surface or to the base contacts. Similar base regrowth processes have been reported[22] in III-V HBT, and are potential means to obtain high current gain in THz InGaAs/InP HBTs.

IV. CONCLUSION

We have simulated the effect of recombination at the base contacts in highly scaled InGaAs/InP DHBTs and have compared simulations to experimental data. Even in the absence of surface recombination, HBTs with 100 nm emitter width and 10 – 30 nm emitter base spacing—dimensions required for ca. 1 THz f_{max} – will show low DC current gain as a result of recombination at the base contacts. Recombination at the base contact becomes progressively larger as the emitter contact width and base-emitter contact spacings are reduced.

ACKNOWLEDGEMENTS

A portion of this work was done in the UCSB nanofabrication facility, part of NSF-funded NNIN network, and MRL Central Facilities supported by the MRSEC Program of the NSF under award No. MR05-20415.

[1] M. J. W. Rodwell, M. Le, and B. Brar, Proc. IEEE **96**, 271 (2008).
[2] T. B. Reed, Z. Griffith, P. Rowell, M. Field, and M. J. W. Rodwell, in *IEEE Compound Semiconductor IC Symposium* (2013).
[3] H.-C. Park, M. Piels, E. Bloch, M. Lu, A. Sivananthan, Z. Griffith, L. Johansson, J. E. Bowers, L. A. Coldren, and M. J. W. Rodwell, in *Proceedings of the European Conference on Optical Fiber Communication* (2013).
[4] V. Jain, J. C. Rode, H. Chiang, A. Baraskar, E. Lobisser, B. J. Thibeault, M. J. W. Rodwell, M. Urteaga, D. Loubychev, A. Snyder, Y. Wu, J. M. Fastenau, and W. Liu, in *Proceedings of the 69th IEEE Device Research Conference* (2011).
[5] M. Urteaga, R. Pierson, P. Rowell, V. Jain, E. Lobissor, and M. J. W. Rodwell, in *Proceedings of the 69th IEEE Device Research Conference* (2011).
[6] P. M. Asbeck, M. -C. F. Chang, J. A. Higgins, N. H. Sheng, G. J. Sullivan, and K.-C. Wang, IEEE Trans. Electron Devices **36**, 2032 (1989).
[7] H.-H. Lin and S.-C. Lee, Appl. Phys. Lett. **47**, 839 (1985).
[8] E. F. Chor, W. K. Chong, and C. H. Heng, J. Appl. Phys. **84**, 2977 (1998).
[9] M. J. W. Rodwell, M. Urteaga, T. Mathew, D. Scott, D. Mensa, Q. Lee, J. Guthrie, Y. Betser, S. C. Martin, R. Smith, S. Jaganathan, S. Krishnan, S. I. Long, R. Pullela, B. Agarwal, U. Bhattacharya, L. Samoska, and M. Dahlström, IEEE Trans. Electron Devices **48**, 2606 (2001).
[10] D. M. Caughey and R. E. Thomas, Proc. IEEE **55**, 2192 (1967).
[11] C. Canali, G. Majni, R. Minder, and G. Ottaviani, IEEE Trans. Electron Devices **22**, 1045 (1975).
[12] M. A. Haase, V. M. Robbins, N. Tabatabaie, and G. E. Stillman, J. Appl. Phys. **57**, 2295 (1985).
[13] H. Kroemer, Solid-State Electron. **28**, 1101 (1985).
[14] V. Palankovski and Q. Rüdiger, *Analysis and Simulation of Heterostructure Devices, Computational Microelectronics* (Springer-Wien, New York, 2004).
[15] C. H. Henry, R. A. Logan, F. R. Merritt, and C. G. Bethea, Electron. Lett. **20**, 358 (1984).
[16] S. Hausser, G. Fuchs, A. Hangleiter, K. Streube, and W. T. Tsang, Appl. Phys. Lett. **56**, 913 (1990).
[17] S. Datta, K. P. Roenkera, M. M. Cahaya, and W. E. Stanchina, Solid-State Electron. **43**, 73 (1999).
[18] E. Zielinski, H. Schweizer, K. Streubel, H. Eisele, and G. Weimann, J. Appl. Phys. **59**, 2196 (1986).
[19] M. Dahlström, "Ultra high speed InP heterojunction bipolar transistors," Ph.D. thesis, Royal Institute of Technology, Stockholm, Sweden, 2003.
[20] G. Zohar, S. Cohen, V. Sidorov, A. Gavrilov, B. Sheinman, and D. Ritter, IEEE Trans. Electron Devices **51**, 658 (2004).
[21] B. Jagannathan, M. Khater, F. Pagette, J.-S. Rieh, D. Angell, H. Chen, J. Florkey, F. Golan, D. R. Greenberg, R. Groves, S. J. Jeng, J. Johnson, E. Mengistu, K. T. Schonenberg, C. M. Schnabel, P. Smith, A. Stricker, D. Ahlgren, G. Freeman, K. Stein, and S. Subbanna, IEEE Electron Device Lett. **23**, 258 (2002).
[22] H. Shimawaki, Y. Amamiya, N. Furuhata, and K. Honjo, IEEE Trans. Electron Devices **42**, 1735 (1995).